ELSEVIER

Journal of Electron Spectroscopy and Related Phenomena 101 (1999) 891–896

JOURNAL OF ELECTRON SPECTROSCOPY and Related Phenomena

Superconducting high-resolution X-ray detectors for metalloprotein L-edge spectroscopy

S. Friedrich[a,c,*], L.J. Hiller[a], M. Frank[a], J.B. le Grand[a], C.A. Mears[a], B. Niderost[a], S.E. Labov[a], A.T. Barfknecht[b], M. LeGros[c], S.P. Cramer[c]

[a]*Lawrence Livermore National Lab, P.O. Box 808, L-418, Livermore, CA 94550, USA*
[b]*Conductus Inc., 969 West Maude Ave., Sunnyvale, CA 94086, USA*
[c]*Lawrence Berkeley National Lab, MS 6-2100, Berkeley, CA 94720, USA*

Abstract

Superconducting tunnel junctions (STJs) can be used as high-resolution energy-dispersive X-ray detectors. STJ detectors are based on the measurement of an increased tunneling current from excess charge carriers that are excited above the superconducting energy gap by the absorption of an X-ray. Nb-based STJ detectors have a theoretical energy resolution limit below 5 eV FWHM for X-ray energies below 1 keV at count rates up to 10 000 counts/s. We have developed Nb–Al–AlOx–Al–Nb X-ray detectors and operated them in a cryostat below 0.4 K in synchrotron experiments. Their resolution varies between 4.6 and 8.9 eV FWHM for X-ray energies between 0.2 and 1 keV. We present fluorescence spectra of metalloproteins and discuss the potential of STJ detectors for fluorescence-detected L-edge absorption spectroscopy of dilute samples.

Keywords: Cryogenic X-ray detectors; Superconducting tunnel junctions; L-edge absorption spectroscopy

1. Introduction

Cryogenic X-ray detectors [1,2] with high energy resolution are being developed for a wide range of applications from material science [3] and micro-analysis [4] to particle [5] and astrophysics [6–8]. The need for low temperature operation arises directly from the desire for better energy resolution. This is ultimately because energy-dispersive detectors in general measure excitations in the detector material and, for a given X-ray energy, a more precise measurement requires smaller excitation energies and less thermal noise.

Superconducting tunnel junctions (STJs) are one class of cryogenic energy-dispersive X-ray detector. They offer very high energy resolution (≈ few eV below 1 keV) at maximum count rates well above those of other cryogenic detectors (≈10 000 counts/s) [9]. STJs consist of two superconducting electrodes separated by a thin insulator. They utilize the small energy gap by which excited single particle states are separated from the Cooper pairs that constitute the superconducting electronic ground state. An X-ray photon absorbed in one of the electrodes breaks Cooper pairs and thereby generates excess charge carriers in proportion to its energy. These charges can tunnel through the insulating barrier, thus producing an increased current proportional to the energy of the incoming X-ray. STJ detectors rely on measuring the excess current after X-ray absorption. As such, their operating principle

*Corresponding author.
E-mail address: sfriedrich@lbl.gov (S. Friedrich)

0368-2048/99/$ – see front matter
PII: S0368-2048(98)00410-1

is similar to that of conventional semiconductor Si(Li) or Ge detectors. One essential difference is that the gap in superconductors is of order 1 meV, about a factor 1000 smaller compared to semiconductors. X-rays therefore generate roughly 1000 times more excess charge carriers in superconductors compared to semiconductors. Theoretically, this results in an improved energy resolution by a factor $\sqrt{1000} \approx 30$. For Nb-based STJs, the statistics of the initial charge generation ultimately limit the resolution to values between 0.8 and 1.7 eV FWHM for X-ray energies between 0.2 and 1 keV [10].

The count rate of STJ detectors is determined by the lifetime of the charge carriers in the junction electrodes. Ideally, excited excess charges from a previous absorption event should have relaxed to their ground state before the STJ detector measures another X-ray. Otherwise, pile-up will start to reduce the detector performance. Typical lifetimes in our superconducting detectors are of order 2–10 μs. This allows STJ detector operation at count rates of around 10 000 counts/s with undiminished energy resolution. Operation at higher rates is possible with somewhat lower resolution due to pile-up [9].

Our LLNL/LBL collaboration is interested in using STJ detectors for L-edge spectroscopy of metallic centers in proteins. Fluorescence-detected absorption spectroscopy has become an important tool for such an analysis of dilute systems [11,12]. The challenge in these types of experiments on dilute samples lies in the fact that the weak fluorescence from transition metal L lines is often buried in the wings of much stronger neighboring lines when conventional lower-resolution detectors are used. For example, Mn containing biological molecules exhibit weak Mn L fluorescence lines at 637 and 649 eV in the wings of a strong oxygen K emission line at 525 eV. Grating spectrometers do have the required energy resolution, but lack the high efficiency necessary to analyze biological samples within a reasonable time.

STJ detectors offer both high energy resolution and high efficiency to measure precision transition metal L edge absorption spectra in a variety of dilute biological samples. In this paper, we discuss their performance and their potential for fluorescence-detected absorption spectroscopy.

2. Theory

We are developing superconducting tunnel junction detectors based on Nb–Al–AlOx–Al–Nb thin-film technology. They consist of a 265 nm bottom Nb film, an Al–AlOx–Al tunnel junction with 50 to 200 nm thick Al electrodes, and a 165 nm top Nb absorber. The devices are fabricated at Conductus Inc. in Sunnyvale, CA, using a modified photolithographic trilayer process [13]. Device sizes vary between 35×35 μm^2 and 200×200 μm^2. Details of this multilayer fabrication process have been published elsewhere [9].

X-rays are captured in the top Nb electrode by photoelectric absorption. The resulting photoelectron relaxes its energy within 1 ns in a complicated cascade involving inelastic electron–electron and electron–phonon scattering and Cooper pair breaking by high-energy phonons. At the end of the cascade about 60% of the X-ray energy has been converted into charge excitations close to the Nb gap energy and about 40% has been converted into sub-gap phonons whose energy is no longer sufficient to break Cooper pairs [10]. When these charges diffuse from the Nb into the adjacent Al layer, where the superconducting gap is lower, they scatter inelastically to the Al gap energy (Fig. 1). This process is called trapping because it confines the charges to a region close to the tunnel barrier [14]. The main purpose of a trapping layer is to separate the absorber and detector function. The Nb absorber can be made thick for efficient absorption, subject to the constraint that the film stress due to lattice mismatch between Nb and Al does not reduce the quality of the AlOx tunneling barrier. The Al traps can be made thin for fast tunneling such that the excess charges can be detected before they again relax into their ground state. The charges in the trap tunnel across the AlOx barrier and thereby provide the current signal.

There are two types of tunneling processes. Charges can tunnel directly from one electrode into the counterelectrode whenever they face empty available states on the opposite side of the tunnel barrier (Fig. 1, process 1). Once they scatter down to the gap energy in the counterelectrode, this direct tunneling process is no longer possible, because

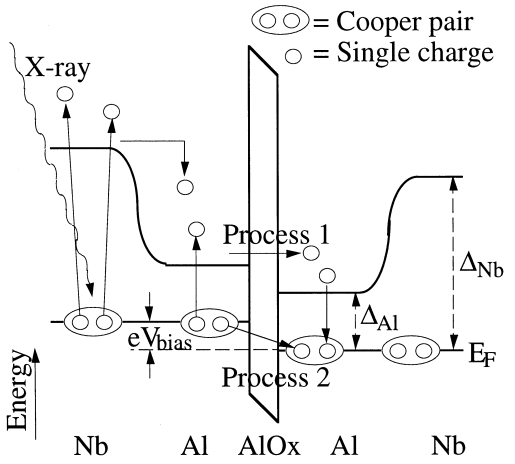

Fig. 1. Energy gap profile $\Delta(x)$ inside a tunnel junction detector. An X-ray breaks Cooper pairs in the Nb absorber thereby generating free single charges, which scatter into the Al trap and produce a current pulse by direct tunneling (process 1) or backtunneling (process 2).

these charges now face the energy gap in the opposing electrode. However, these charges can still contribute to the tunneling current by breaking a Cooper pair in the opposing electrode and forming a new pair with one of the now unpaired electrons in the counterelectrode (Fig. 1, process 2). This process (called backtunneling) moves a charge in the same direction across the tunneling barrier as the direct tunneling process, while returning an unpaired particle back to the other electrode. Both processes occur at the same tunneling rate $1/\tau_{tunn}$. Charges can engage in both tunneling processes until they ultimately recombine and form Cooper pairs again after a characteristic recombination time τ_{rec}. Backtunneling therefore provides an intrinsic charge amplification by a factor given by the average number of tunneling events τ_{rec}/τ_{tunn} each charge carrier undergoes. Since the number of tunneling events is subject to statistical fluctuations, this charge amplification process also adds statistical noise to the tunneling current [15]. Since backtunneling increases the both the signal and the noise, it is desirable in STJ detectors only as long as the electronic noise contributes an appreciable fraction to the resolution. Once the electronic noise is negligible, backtunneling reduces the ultimate detector resolution and should be suppressed. The devices discussed in this paper amplify the signal by a factor 3.1 through backtunneling. This degrades the ultimately attainable linewidth to 2.0–4.6 eV for X-ray energies between 0.2 and 1 keV.

3. Experimental results

The STJ detectors are operated in a liquid helium cryostat with an adiabatic demagnetization refrigerator (ADR) stage. It attains a base temperature of 60 mK and can be attached to a synchrotron beam line. The ADR has a hold time of 4–6 h below 0.4 K and requires about 30 min to cycle. Note that the temperature does not need to be regulated. We typically operate the STJ in two different modes. For detector characterization, we illuminate the STJ detector directly with a monochromatic beam from a low-flux beam line. For fluorescence experiments, we insert a sample stage through a load lock to within 5 mm of the STJ detector. A single 200×200 μm^2 detector then covers a solid angle $\Omega=1.6\cdot10^{-3}$ sr. For details of the experimental setup, see Refs. [3] and [10].

Fig. 2 shows the response of a 50×50 μm^2 STJ detector at an incident energy of 400 and 800 eV. The resolution, as determined from a Gaussian fit to the main peak, is 5.4 eV FWHM at 400 eV, with a noise contribution of 3.9 eV from the readout electronics. At energies below $\approx$600 eV the detector response almost Gaussian and free from artifacts. Above $\approx$600 eV a certain fraction of the X-rays are absorbed in the bottom Nb electrode. Since the two electrodes can have a slightly different response function, the lines can appear broadened or split (see 800 eV line). These data were obtained by direct illumination at the Stanford Synchrotron Radiation Laboratory, beam line 1-1. The low energy background events are due to scattered white light from the monochromator.

The inset in Fig. 2 shows the detector resolution as a function of energy. It varies between 4.6 and 8.9 eV in the X-ray band between 0.2 and 1 keV. We can subtract the electronic noise and the monochromator line width in quadrature from the measured resolution to obtain the intrinsic detector resolution. The

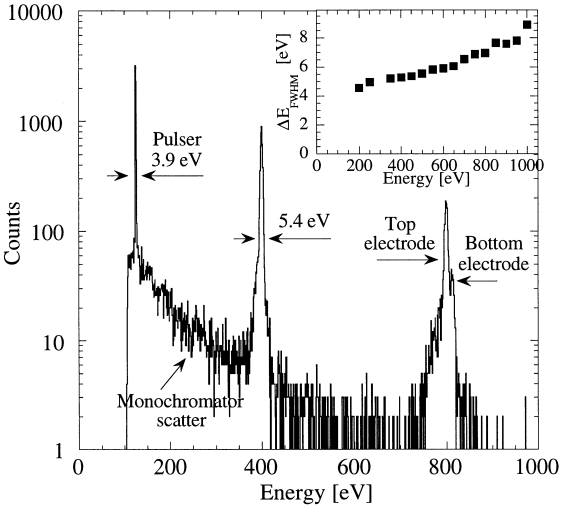

Fig. 2. STJ response to monochromatic 400 and 800 eV X-ray photons. Above ≈600 eV, the lines appear split due to absorption in the bottom Nb electrode. The inset shows the detector resolution as a function of energy.

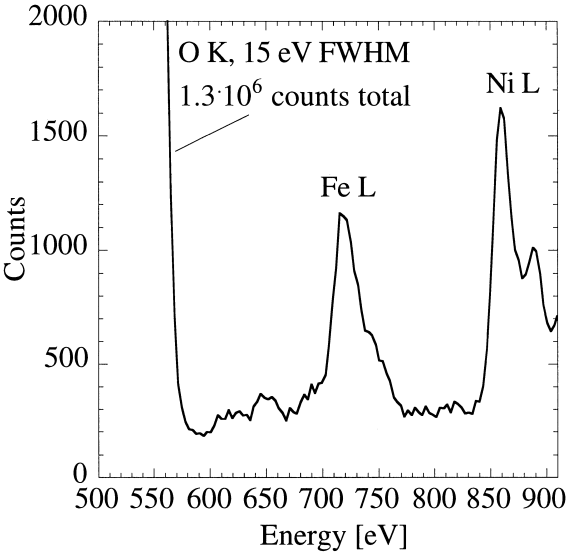

Fig. 3. Fluorescence spectrum of the hydrogenase protein from the bacterium *D. gigas*.

intrinsic resolution approaches the theoretical limit to within 15% [16]. We believe that this small discrepancy is due to X-ray absorption in the spatially inhomogeneous Nb/Al bilayer, while the calculations of the theoretical limit assume X-ray absorption in a homogeneous superconductor. This experiment shows that STJ detector technology is mature enough to be used in various fluorescence applications.

Fig. 3 shows a fluorescence spectrum of hydrogenase, an enzyme from the bacterium *Desulfovibrio gigas* that is responsible for hydrogen evolution and uptake [17]. The sample contains about 500 ppm Ni and 12 times more Fe. The spectrum was acquired with a 200×200 μm^2 detector with a resolution of 15 eV FWHM at 525 eV. Its resolution is lower than the resolution of the 50×50 μm^2 detector shown in Fig. 2 due to its higher device capacitance. It is still sufficient to fully separate the Ni L and the Fe L fluorescence from the strong oxygen K line centered at 525 eV. Both lines appear split for reasons explained above. The Fe line intensity does not reflect the 12:1 abundance ratio of Fe to Ni, because Fe is excited less efficiently by the incident radiation, and because residual gases frozen out on the sample attenuate the Fe signal more strongly than the higher-energy Ni fluorescence. The background events are due to scattered white light from the monochromator. A detector with a resolution shown in Fig. 3 is sufficient to separate weak Mn L lines from nearby oxygen K fluorescence. This measurement demonstrates the potential of STJ detectors for fluorescence-detected absorption spectroscopy of Mn L-edges in dilute samples.

4. Discussion and future work

We now estimate the performance of STJ detectors in fluorescence-detected absorption spectroscopy of dilute samples. As an example, we consider the oxygen-evolving protein photosystem II (PSII) which contains roughly 100 ppm Mn. There is presently considerable interest in better determining the oxidation state of the central four Mn atoms as the protein changes its state within the catalytic cycle [18]. To a first approximation, the Mn L fluorescence flux from PSII measured in a detector covering a solid angle $\Omega/4\pi$ is given by [11]

$$I_F \approx I_0 \frac{\epsilon_{MnL}\mu_{Mn}(E_0)}{\mu_t(E_0)+\mu_t(E_F)}\cdot\frac{\Omega}{4\pi}$$

Here I_0 is the incident X-ray flux, μ_{Mn} is the linear

absorption coefficient of Mn and μ_t is the total linear absorption coefficient of the sample at incident energy E_0 and fluorescence energy E_F, respectively [19], and ϵ_{MnL} is the fluorescence yield of a vacancy in the Mn L shell [20]. Under ideal conditions, the count rate in a single 200×200 μm^2 STJ detector located at a distance of 5 mm from the PSII sample will be roughly 5 counts/s for an incident flux $I_0=10^{10}$ photons/s. If the background at the Mn L energies around 640 eV is dominated by scattered white light from the monochromator (cf. Fig. 3), the background count rate will be of order 2 counts/s. A single fluorescence spectrum with a signal-to-noise ratio of 10 can then be acquired within 30 s. An absorption spectrum in which the incident X-ray energy is scanned through the Mn L absorption edge will take less than an hour. Averaging several spectra may be desirable to further increase the signal-to-noise ratio.

At present, there are three main limitations to our STJ detector system. The first is due to the line splitting artifact above 600 eV (Figs. 2, 3). For fluorescence-detected absorption spectroscopy this may be tolerable, as long as there is no confusion about the origin of the second line and it is well separated from all other lines. However, in spectra of unknown samples the line splitting may lead to ambiguities. Future devices will employ Ta rather than Nb absorbers for higher efficiencies at higher energies.

The second difficulty arises from the need to operate the STJ detector below 0.4K. While the cooling of the detector in an adiabatic demagnetization refrigerator with 60 mK base temperature is straightforward, operating the detector requires IR blocking windows between the beam line and the cold sample and detector to prevent 300 K radiation from heating the detector. Under present vacuum conditions (10^{-7} Torr range), residual gases freezing out on the windows can reduce the incident flux by as much as a factor of 10 and increase the required data acquisition time accordingly. In the future, we will improve the vacuum conditions and re-design the cryostat such that fewer windows have to be used.

The third limitation is due to the small detector size. We are currently developing 3-by-3 arrays to increase the solid angle by an order of magnitude to $1.5\cdot10^{-2}$ sr. Future experiments will also use X-ray focusing optics to further increase the detector efficiency [4].

5. Summary

We have developed superconducting tunnel junction (STJ) X-ray spectrometers for L-edge spectroscopy of biological samples. They have an energy resolution between 4.6 and 8.9 eV FWHM for X-ray energies between 0.2 and 1 keV at count rates up to $\approx$10 000 counts/s. Our STJ detectors can completely separate weak transition metal L-lines from strong nearby carbon and oxygen K-lines. This will improve the sensitivity of fluorescence-detected absorption spectroscopy of metalloproteins in synchrotron-based experiments.

Acknowledgements

We thank Jan Batteaux and Jeff Moore for expert technical assistance and Daulat Patil for providing the hydrogenase samples. This work was performed under the auspices of the US Department of Energy by LLNL under contract No. W-7405-ENG-48 at the Stanford Synchrotron Radiation Laboratory (SSRL) which is operated by the DoE, Office of Basic Energy Sciences. Funding for this research was provided by the DoE, Office of Biological and Environmental Research, by the NIH through grant No. GM 44380, and by NASA through SBIR Contract No. NAS5-32805 and through UV detector development grant No. NAG5-4137.

References

[1] N.E. Booth, D.J. Goldie, Supercond. Sci. Technol. 9 (1996) 493.
[2] D. Twerenbold, Rep. Prog. Phys. 59 (1996) 349.
[3] M. Frank, C.A. Mears, S.E. Labov, L.J. Hiller, J.B. LeGrand, M.A. Lindeman, H. Netel, D. Chow, A.T. Barfknecht, J. Synchrotron Rad. 5 (1998) 515.
[4] D.A. Wollman, K.D. Irwin, G.C. Hilton, L.L. Dulcie, D.E. Newbury, J.M. Martinis, J. Microsc. 188 (1997) 196.
[5] S.W. Nam, B. Cabrera, B. Chugg, R.M. Clarke, C. Fertig,

K.D. Irwin, B.A. Young, Nucl. Instrum. Methods A370 (1996) 187.
[6] D. McCammon, R. Almy, S. Deiker, J. Morgenthaler, R.L. Kelley, F.J. Marshall, S.H. Moseley, C.K. Stahle, A.E. Szymkowiak, Nucl. Instrum. Methods A370 (1996) 266.
[7] S. Friedrich, K. Segall, M.C. Gaidis, C.M. Wilson, D.E. Prober, P.J. Kindlmann, A.E. Szymkowiak, S.H. Moseley, IEEE Trans. Appl. Superconduct. 7 (1997) 3383.
[8] A. Peacock, P. Verhoeve, N. Rando, A. van Dordrecht, B.G. Taylor, C. Erd, M.A.C. Perryman, R. Venn, J. Howlett, D.J. Goldie, L. Lumley, M. Wallis, Nature 381 (1996) 135.
[9] M. Frank, L.J. Hiller, J.B. LeGrand, C.A. Mears, S.E. Labov, M.A. Lindeman, H. Netel, D. Chow, A.T. Barfknecht, Rev. Sci. Instrum. 69 (1998) 25.
[10] N. Rando, A. Peacock, A. van Dordrecht, C.L. Foden, R. Engelhard, B.G. Taylor, P. Gare, J. Lumley, C. Pereira, Nucl. Instrum. Methods A 313 (1992) 173.
[11] J. Jaclevic, J.A. Kirby, M.P. Klein, A.S. Robertson, G.S. Brown, P. Eisenberger, Solid State Commun. 23 (1977) 679.
[12] S.P. Cramer, J. Chen, S.J. George, J. van Elp, J. Moore, O. Tench, J. Colaresi, M. Yocum, O.C. Mullins, C.T. Chen, Nucl. Instrum. Methods A319 (1992) 285.
[13] A.T. Barfknecht, R.C. Ruby, H. Ko, IEEE Trans. Magn. 27 (1991) 970.
[14] N.E. Booth, Appl. Phys. Lett. 50 (1987) 293.
[15] C.A. Mears, S.E. Labov, A.T. Barfknecht, Appl. Phys. Lett. 63 (1993) 2961.
[16] J.B. LeGrand, C.A. Mears, L.J. Hiller, M. Frank, S.E. Labov, H. Netel, D. Chow, S. Friedrich, M.A. Lindeman, A.T. Barfknecht, Appl. Phys. Lett. 73 (1998) 1.
[17] J.R. Lancaster (Ed.), The Bioinorganic Chemistry of Nickel, VCH, New York, 1988.
[18] V.K. Yachandra, K. Sauer, M.P. Klein, Chem. Rev. 96 (1996) 2927.
[19] For numerical values, see http://www-cxro.lbl.gov/optical_constants/
[20] M.O. Krause, J. Phys. Chem. Ref. Data 8 (1979) 307.